

High-density racetrack memory based on magnetic skyrmion bags controlled by voltage gates

Cite as: J. Appl. Phys. **132**, 113901 (2022); <https://doi.org/10.1063/5.0098999>

Submitted: 11 July 2022 • Accepted: 25 August 2022 • Published Online: 16 September 2022

 Zhiyu Zhang,  Min Xu,  Guiqian Jiang, et al.



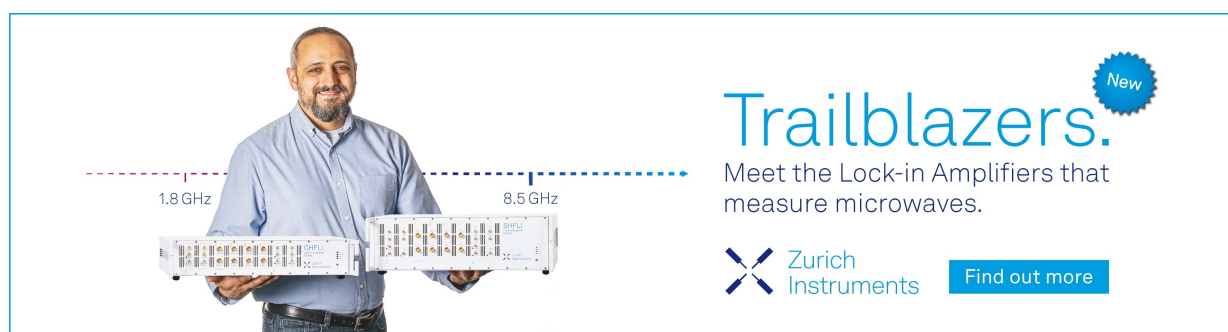
View Online




Export Citation




CrossMark



Trailblazers. 

Meet the Lock-in Amplifiers that measure microwaves.

 Zurich Instruments [Find out more](#)

High-density racetrack memory based on magnetic skyrmion bags controlled by voltage gates

Cite as: J. Appl. Phys. **132**, 113901 (2022); doi: [10.1063/5.0098999](https://doi.org/10.1063/5.0098999)

Submitted: 11 July 2022 · Accepted: 25 August 2022 ·

Published Online: 16 September 2022



Zhiyu Zhang,  Min Xu,  Guiqian Jiang,  Jinyu Zhang,  Dexiang Meng,  Wenlong Chen,  Yuliang Chen,  and Changjing Hu 

AFFILIATIONS

Key Laboratory for Anisotropy and Texture of Materials (MOE), School of Materials Science and Engineering, Northeastern University, Shenyang 110819, China

^{a)}Author to whom correspondence should be addressed: xum@smm.neu.edu.cn

ABSTRACT

Skyrmion bags are spin structures with arbitrary topological degrees. They are expected to be promising next-generation information carriers due to their inherent high topological degrees. Here, we report the dynamics of the topological transition process when a skyrmion bag passes through a voltage gate driven by spin current in a synthetic antiferromagnetic racetrack with voltage-controlled magnetic anisotropy. The topological degrees of skyrmion bags controlled by voltage gate and driving current density are investigated. It is found that the different topological degrees of skyrmion bags transformed in this process are related to the interaction between antiskyrmions inside skyrmion bags, and the energy of each inner antiskyrmion after topological transformation is on the order of 10^{-19} J. Furthermore, we have realized the successive transition of a skyrmion bag from a high topological degree to a low topological degree on a racetrack with three voltage gates. This work is helpful for designing high-density racetrack memory and logical devices based on skyrmion bags.

Published under an exclusive license by AIP Publishing. <https://doi.org/10.1063/5.0098999>

I. INTRODUCTION

Magnetic skyrmions,^{1–5} as topologically protected magnetization configurations with particle-like properties, were first experimentally observed in 2009.⁶ Due to their stability, nanoscale size, and low driving current density, skyrmions are considered as promising candidates in the next generation of spintronic devices, such as racetrack memories,^{7–11} nano-oscillators,^{12–14} and other logical devices.^{15–20} Some experiments have revealed that skyrmions can be generated and driven by electric current at room temperature, which enhances the application prospects of skyrmions as information carriers.^{2,3,21}

However, when skyrmions are applied to racetrack memory, one skyrmion can only represent one bit and the repulsion between skyrmions keeps them at a relatively long distance,^{22,23} which is not conducive to high-density information storage. Moreover, the defects in ferromagnetic materials may lead to data loss. Since 2019, attention has been drawn to the skyrmion bags, which not only retain the advantages of a single skyrmion but also encode more information for each topological structure.^{21,23}

Skyrmion bags are nested skyrmionic structures with a high degree of freedom of topological charge numbers.^{24,25} They are composed of a single skyrmion outer boundary and a number of inner antiskyrmions, which enables them to represent different information with different topological charges. In recent research, skyrmion bags have been proposed as carriers of high-density information and they can move along nanotracks driven by spin current, just like skyrmions. In addition, skyrmion bags exhibit good topological protection when passing through defects, which makes them have greater advantages in applications to the racetrack memory.²³

Skyrmion bags can be characterized by the total topological charge number, i.e., topological degree,^{23,24} as

$$Q = \frac{1}{4\pi} \int \mathbf{m} \cdot (\partial_x \mathbf{m} \times \partial_y \mathbf{m}) dx dy, \quad (1)$$

where \mathbf{m} is the unit vector field of magnetization. According to this definition, for a skyrmion, $Q = -1$, and for an antiskyrmion,

$Q = +1$. We use the notation $S(N)$ to describe skyrmion bags composed of a number of antiskyrmions inside the outer skyrmion, where N is the number of inner antiskyrmions, and the total topological degree is $Q = N - 1$.^{24,26} In other words, $S(0)$ is a single skyrmion, and $S(N)$ ($N > 0$) represents the skyrmion bags with N inner antiskyrmions.

In this paper, we have demonstrated that the high-density racetrack memory based on skyrmion bags can be realized in a synthetic antiferromagnetic racetrack with voltage-controlled perpendicular magnetic anisotropy (VCMA). We have found that the topological degree of a skyrmion bag can be modulated by the length of the voltage gate, perpendicular magnetic anisotropy (PMA) gradient in the voltage gate and driving current density. The topological transitions of a skyrmion bag occur from initial state $S(4)$ to $S(N)$ ($N = 1-4$) when the skyrmion bag passes through the voltage gate, so $S(N)$ can represent two binary bits 00, 01, 10, and 11, respectively, which helps to store more information at one time. Moreover, we have explored the reasons for different topological transitions, such as the interaction forces between inner antiskyrmions. Finally, in order to extend our design idea, we try to achieve a continuous transition from $S(4)$ to $S(3)$ to $S(2)$ to $S(1)$ by placing three voltage gates on a racetrack. These results will contribute to the realization of high-density memory and logical devices based on skyrmion bags.

II. MODEL AND METHODS

Our work is performed by micromagnetic simulations using OOMMF code.²⁷ The dynamics of the magnetization of the system is numerically calculated by the Landau-Lifshitz-Gilbert (LLG) equation with spin transfer torques as follows:²⁸

$$\frac{d\mathbf{m}}{dt} = -\gamma_0 \mathbf{m} \times \mathbf{H}_{\text{eff}} + \alpha \left(\mathbf{m} \times \frac{d\mathbf{m}}{dt} \right) - (\mathbf{u} \cdot \nabla) \mathbf{m} + \beta \mathbf{m} \times [(\mathbf{u} \cdot \nabla) \mathbf{m}], \quad (2)$$

where $\mathbf{m} = \mathbf{M}/M_s$, M_s is the saturation magnetization, γ_0 is the absolute value of the gyromagnetic ratio, α is the Gilbert damping coefficient, β is the non-adiabatic spin-transfer parameter, and \mathbf{u} is the spin current velocity. The effective field is computed by $\mathbf{H}_{\text{eff}} = -\frac{1}{\mu_0 M_s} \frac{\delta E}{\delta \mathbf{m}}$, where E is the total energy which consists of the exchange, Dzyaloshinskii-Moriya interaction (DMI), uniaxial anisotropy, demagnetization, and Ruderman-Kittel-Kasuya-Yosida (RKKY) energy.

In our simulations, the mesh size is set as $2 \times 2 \times 1 \text{ nm}^3$, which is small enough to ensure the accuracy of the calculations. The magnetic parameters are as follows:^{1,23,29} $M_s = 580 \text{ kA/m}$, PMA constant $K_u = 0.8 \text{ MJ/m}^3$, interfacial DMI constant $D = 3.5 \text{ mJ/m}^2$, Heisenberg exchange constant $A = 15 \text{ pJ/m}$, $\alpha = 0.3$, $\beta = 0.4$, and bilinear interfacial exchange coefficient $\sigma = -2 \times 10^{-3} \text{ J/m}^2$. The spin current velocity $\mathbf{u} = g\mu_B P/2eM_s$, where J is the electrical current density, g is the Landé factor, μ_B is the Bohr magneton, e is the electron charge, and the spin polarization P is 0.4.

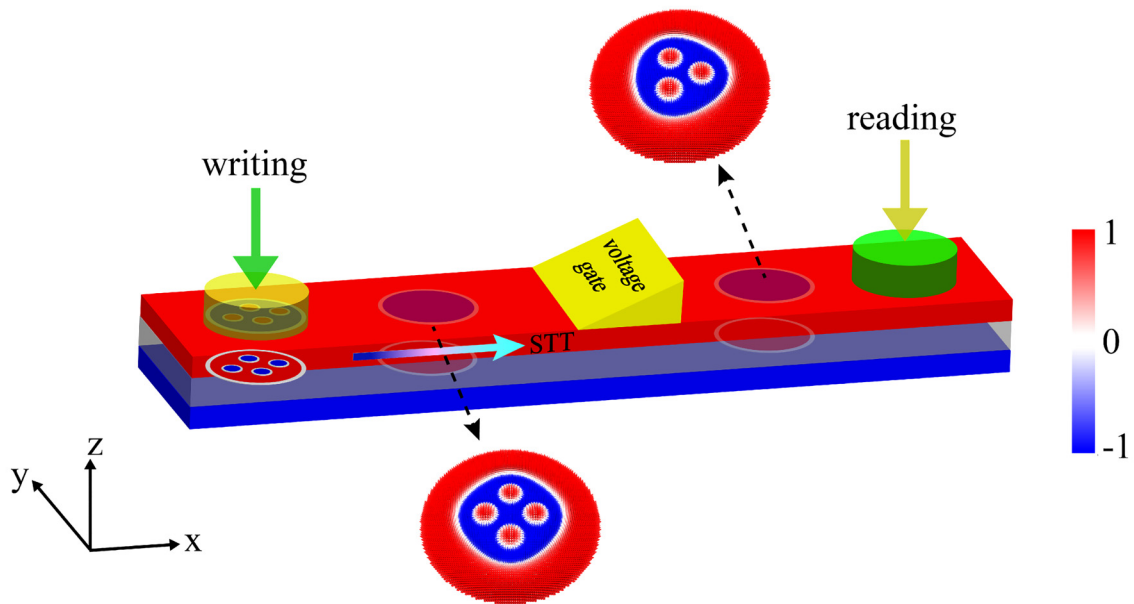
III. RESULTS AND DISCUSSION

Figure 1(a) shows our simulation model of three-layer structure based on a skyrmion bag, containing two ferromagnetic layers of $600 \times 200 \times 1 \text{ nm}^3$ and a middle insulating layer. In this system, the strong antiferromagnetic coupling between the top and the bottom layers leads to the mutual cancellation of Magnus forces acting on the skyrmion bag. Therefore, the trajectory of the skyrmion bag driven by the spin transfer torque (STT) does not deviate longitudinally. For convenience, we only show the snapshots of the skyrmion bag at the top level in the following discussion.

An outer skyrmion can be created by an electric potential from a non-magnetic scanning tunneling microscope (STM) tip,³⁰ then forced to grow under a fine magnetic field, and then inner antiskyrmions can be generated within the bigger skyrmion by an electric field.²² In our simulation, for convenience, the magnetization of the top layer is initially set to $m_z = 1$, and a circle with a radius of 60 nm and $m_z = -1$ is set at the place 100 nm away from the left end of the racetrack as the writer, in which four circles with a radius of 10 nm and $m_z = 1$ are set, and then relaxed for 1 ns to form the original skyrmion bag $S(4)$. $S(4)$ moves toward the right side of the racetrack driven by STT. A wedge-shaped voltage gate is set in the middle of the ferromagnetic racetrack. The PMA constant $K_v(x)$ in the voltage gate can be expressed as¹⁵ $K_v(x) = K_u + (K_{uv} - K_u)(x - x_0)/L$ for $x \in [x_0, x_0 + L]$, where K_{uv} is the maximum PMA, L is the length, and x_0 is the position of the gate. Therefore, the length of the voltage gate and PMA gradient in the gate can be modulated by changing L and K_{uv} , respectively, which helps us conveniently adjust the topological number of the skyrmion bag in the voltage gate. The anisotropy curve along the racetrack is given in Fig. S1 in the [supplementary material](#). Furthermore, the local magnetoresistance changes in the vicinity of skyrmion³¹ can be read by tunneling spin-mixing magnetoresistance (TXMR) utilizing a non-magnetic STM tip, which has the potential to “read” skyrmion and can be extended to read the skyrmion bags $S(N)$ ($N = 1-4$).²² In Fig. 1(b), the size and shape of the outer skyrmion of the skyrmion bag vary with the increase of the number of inner antiskyrmions, but the size of inner antiskyrmions remains almost constant. Interestingly, the different arrangements of inner antiskyrmions have no or slight effect on the total energy of skyrmion bag $S(N)$, which is negligible in our simulation, shown in Fig. S2 in the [supplementary material](#).

The number of inner antiskyrmions decreases gradually with the increase of the gate length L under a specific K_{uv} , exhibited in Fig. 2(a). The reason for the change is that with the increase of L , the skyrmion bag takes longer to pass through the voltage gate, and its size gradually shrinks due to the high PMA in the voltage gate, which makes the inner antiskyrmions easier to be annihilated. When K_{uv} is kept at 1.12 MJ/m^3 , the passing time of skyrmion bag rises as L increases, as shown in Fig. 2(c). Figure 2(b) illustrates that the increase of driving current density helps inner antiskyrmions pass through the voltage gate, which is also revealed in Fig. 2(c), in which the passing time of skyrmions bags decreases with the increase of J when K_{uv} is 1.12 MJ/m^3 . In addition, the increase of K_{uv} enhances not only the average value of PMA, but also the PMA gradient in the voltage gate, and both contribute to

(a)



(b)

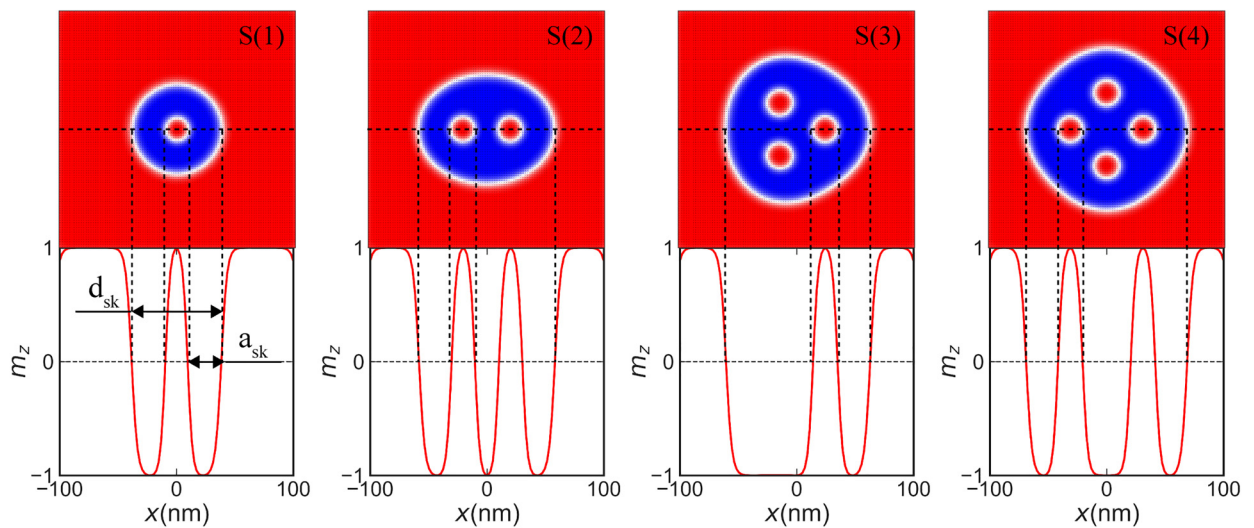


FIG. 1. (a) Schematic diagram of a racetrack memory device based on a skyrmion bag controlled by a voltage gate. (b) Magnetization distributions of skyrmion bags $S(N)$ ($N = 1-4$) in the steady state and the corresponding out-of-plane magnetization components (m_z), in which d_{sk} is the size of the outer skyrmion along the x axis and a_{sk} is the diameter of the inner antiskyrmion.

the annihilation of inner antiskyrmion. In Fig. 2(d), both skyrmion bags are subjected to the driving force (F_j) and resistance (F_{R1} or F_{R2}) induced by the PMA gradient in the voltage gate, where $F_R \propto \partial K_v / \partial x$.³² The size of antiskyrmions in the skyrmion bag with larger K_{uv} is smaller than that in the skyrmion bag with smaller K_{uv} because $K_{uv1} < K_{uv2}$ and $F_{R1} < F_{R2}$.

In Fig. 3(a), a relaxed skyrmion bag $S(4)$ at $x = -200$ nm on the racetrack is used as the initial state and the adjacent inner antiskyrmions in the skyrmion bag have the same size and spacing, where the four inner antiskyrmions are marked as a_1 , a_2 , a_3 , and a_4 counterclockwise and the force analysis of a_4 is also shown. The repulsive forces on a_4 come from the other three inner

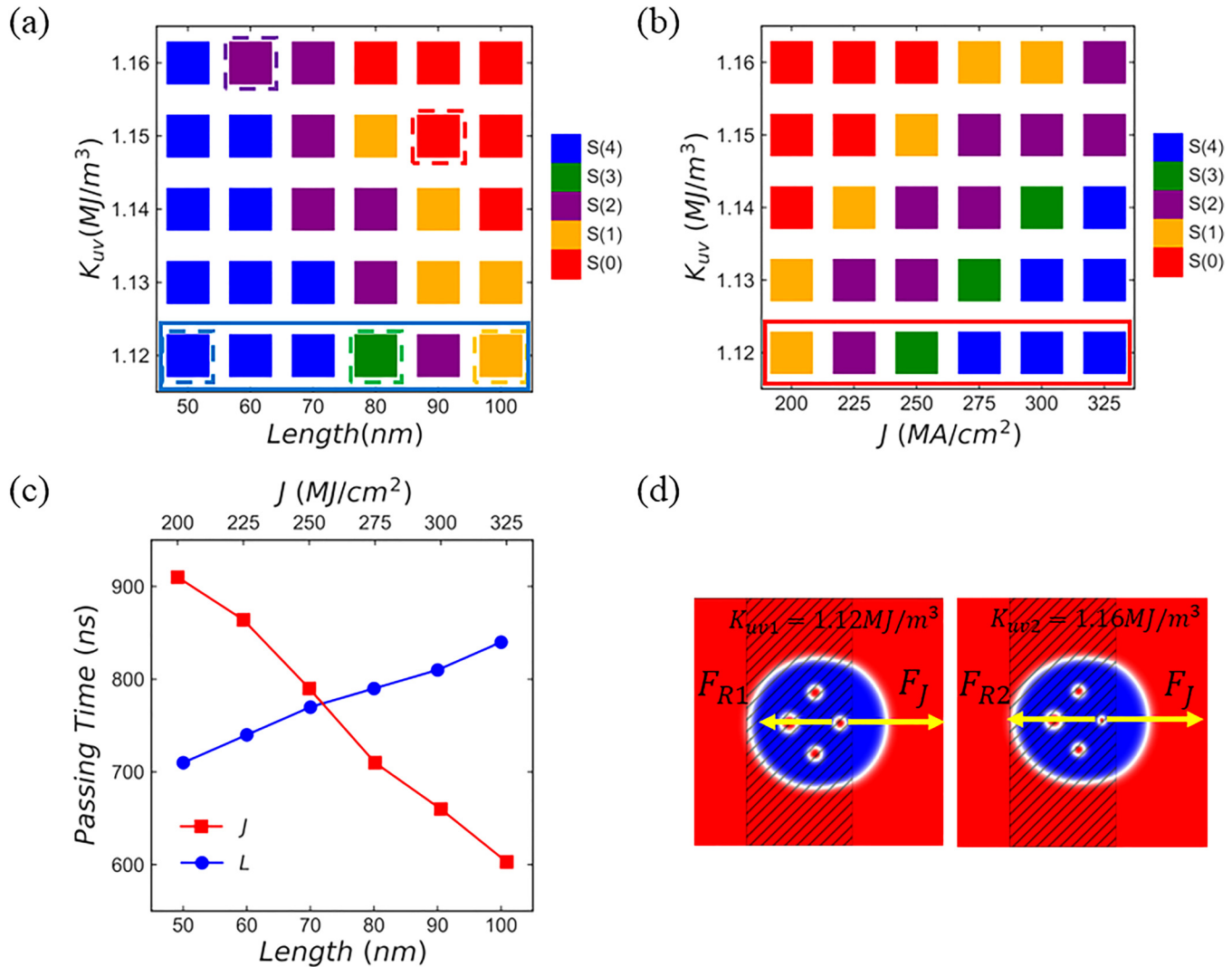


FIG. 2. (a) State diagram of a skyrmion bag with initial state S(4) after passing through a voltage gate with $L = 50\text{--}100$ nm and $K_{uv} = 1.12\text{--}1.16$ MJ/m³ driven by a current of $J = 250$ MA/cm². (b) State diagram of a skyrmion bag with initial state S(4) after passing through a voltage gate with $L = 80$ nm and $K_{uv} = 1.12\text{--}1.16$ MJ/m³ driven by a current of $J = 200\text{--}325$ MA/cm². (c) The passing time of a skyrmion bag S(4) as a function of L and J under the conditions of the states framed with solid lines in Figs. 2(a) and 2(b). (d) The driving force F_J induced by STT ($J = 250$ MA/cm²) and the resistance forces F_{R1} and F_{R2} induced by PMA gradient in the voltage gate with $L = 80$ nm, $K_{uv1} = 1.12$ MJ/m³, and $K_{uv2} = 1.16$ MJ/m³, respectively.

antiskyrmions and the outer skyrmion, expressed as F_1 , F_2 , F_3 , and F_0 , respectively, where $|F_1| = |F_3| > |F_2|$, considering the distances between a_1 , a_2 , and a_3 from a_4 . In addition, the outer skyrmion provides a_4 with a force F_0 to keep it in equilibrium inside the skyrmion bag, where $F_0 = -(F_1 + F_2 + F_3)$. Since the other three inner antiskyrmions are also in equilibrium, S(4) moves stably in the $+x$ direction as a whole driven by the STT. However, the skyrmion bag cannot remain stable when entering the voltage gate. The inner antiskyrmion a_4 is subjected to the combined forces of $F_1 + F_2 + F_3$, which contribute to pushing it away from the voltage gate. Therefore, if a_4 annihilates inside the voltage gate, the

other inner antiskyrmions cannot pass, as shown in Fig. 3(b). The size of a_4 rises rapidly after leaving the voltage gate, which increases the repulsive forces F_4 of a_4 to the other inner antiskyrmions, resulting in the shrinking and annihilation of a_1 , a_3 and a_2 when they approach the right end of the voltage gate with $L = 100$ nm, illustrated in Fig. 3(c).

In Fig. 3(d), a_1 and a_3 are in the same position along the x axis direction, which makes them both subject to the same magnitude of repulsive forces from the other inner antiskyrmions and the same magnitude of PMA, so they either pass through the voltage gate or annihilate at the same time. S(4) tends to convert into S(2)

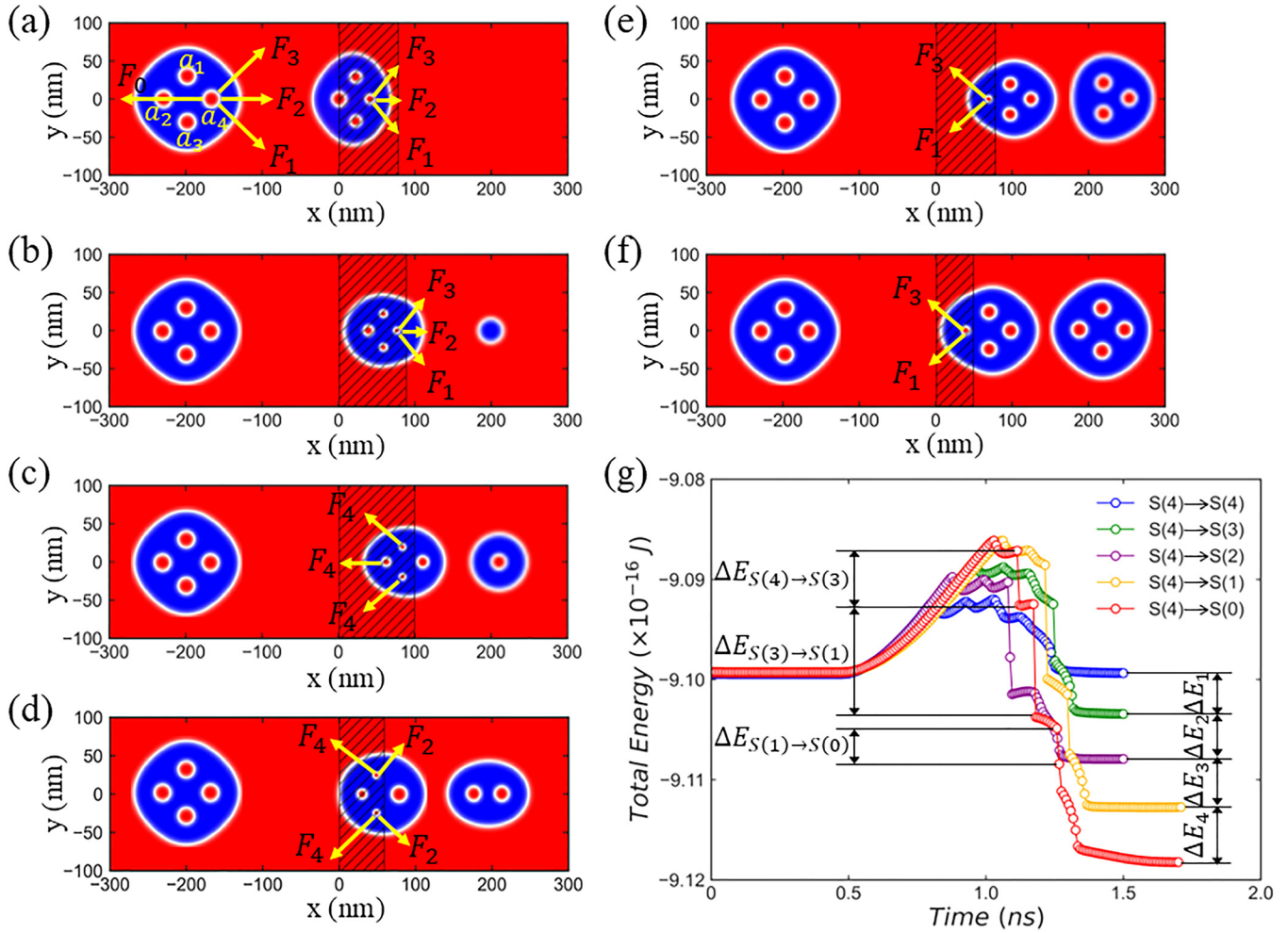


FIG. 3. (a) Schematic diagram of the forces on inner antiskyrmions when skyrmion bag S(4) entering the voltage gate with $L = 80$ nm and $K_{uv} = 1.12$ MJ/m³. F_i ($i = 0 - 3$) denotes the repulsive force from inner antiskyrmion or outer skyrmion. (b)–(f) Schematic diagrams of the forces on inner antiskyrmions when skyrmion bag S(4) leaving the voltage gate to form S(N) ($N = 0-4$), respectively, under the conditions of the states framed with dashed lines in Fig. 2(a). (g) Energy variations of the skyrmion bag S(4) moving on racetracks with different voltage gates to form S(N) ($N = 0-4$) corresponding to Figs. 3(b)–3(f), respectively. The energy gaps between S(4) and S(3), S(3) and S(2), S(2) and S(1), and S(1) and S(0) are denoted as $\Delta E_1, \Delta E_2, \Delta E_3$, and ΔE_4 , respectively. ($\Delta E_1 = 4.07 \times 10^{-19}$ J, $\Delta E_2 = 4.50 \times 10^{-19}$ J, $\Delta E_3 = 4.80 \times 10^{-19}$ J, and $\Delta E_4 = 5.49 \times 10^{-19}$ J).

when it passes through the voltage gate with a shorter L and a larger K_{uv} , where both a_2 and a_4 are comparatively large, so their repulsive forces on a_1 and a_3 should not be ignored. Consequently, a_1 and a_3 are compressed by a_2 and a_4 and annihilated in the voltage gate. In Figs. 3(e) and 3(f), a_1 and a_3 pass through the voltage gate, and a_2 is affected by the repulsive forces from a_1 and a_3 . If $F_1 + F_3$ is small enough, a_2 will pass through the gate, otherwise it will be annihilated in the gate.

In Fig. 3(g), under a driving current of $J = 250$ MA/cm², the energy of the skyrmion bag gradually increases after entering the voltage gate until it reaches a maximum, which is due to the increase of PMA in the voltage gate. As K_{uv} and L of the voltage

gate are different, S(4) undergoes different transitions from S(4) to S(N) ($N = 0-4$) when passing through the voltage gate, in which each topological transition is accompanied by one or more sudden drops of energy. After leaving the voltage gate, the skyrmion bags with a certain topological number reach a stable state with almost constant energy, but the skyrmion bags with different topologies have different energy. It can be found that in the steady state, the size of the antiskyrmions in the skyrmion bags with different topologies is almost identical. Considering the order of the energy gap ΔE_i ($i = 1-4$) between S(N) and S(N-1) ($N = 1-4$), the energy of each inner antiskyrmion is on the order of 10^{-19} J. This is much lower than that of a skyrmion ($\sim 10^{-16}$ J), calculated by integrating

the energy density in the circle of the radius of skyrmion, which is possibly because an antiskyrmion in the skyrmion bag is much smaller than that of a skyrmion under the same conditions.

In order to extend the design idea of high-density information storage based on skyrmion bags, we try to realize a continuous transition from S(4) to S(3) to S(2) to S(1) by designing three voltage gates on a racetrack. In Fig. 4(a), the transitions from S(4) to S(N) ($N=0-4$) can be achieved by increasing K_{uv} , which leads to an increase of PMA gradient in the voltage gate. However, the transition from S(3) to S(1) or S(2) to S(1) cannot occur when the original topological structure is S(3) or S(2). Since there is no

horizontal repulsive force between the vertically aligned inner anti-skyrmions, the transition from S(2) to S(1) cannot happen. Therefore, we have designed three voltage gates with the same K_{uv} and L on a racetrack, in which the height of gate1 and gate2 is 200 nm and the height of gate3 is 100 nm.

In Fig. 4(b), the original skyrmion bag S(4) is generated at $x = -300$ nm and driven by a current of $J = 250$ MA/cm² in the $+x$ direction. When S(4) passes through gate1, the inner antiskyrmion a_2 is annihilated by the repulsive forces $F_1 + F_3$ from a_1 and a_3 in gate1 with high PMA, which is consistent with our previous analysis. However, the situation of S(3) passing through gate2 is

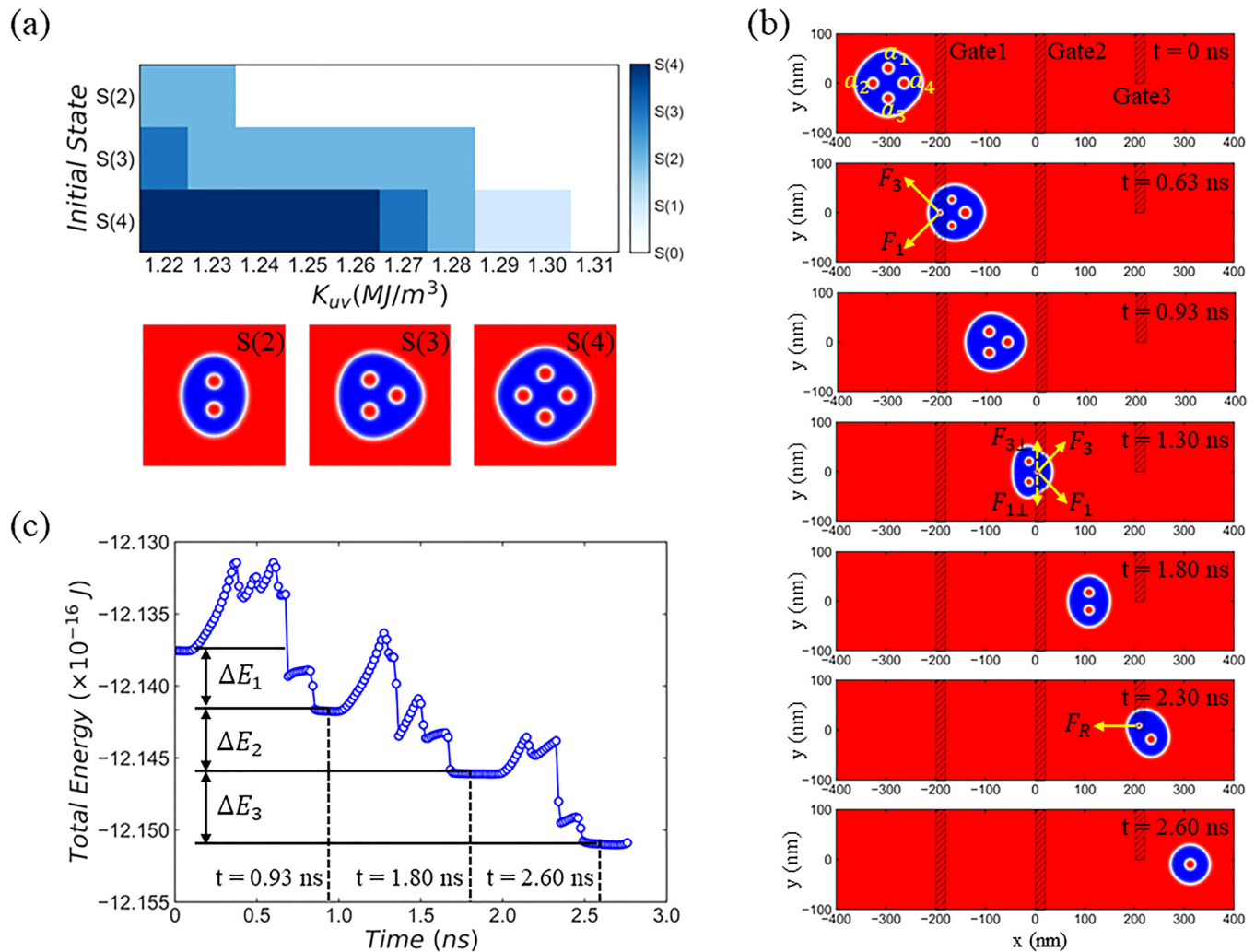


FIG. 4. (a) State diagram of the stable skyrmion bags S(N) ($N=0-4$) formed after different initial bags [S(2), S(3) and S(4)] passing through the voltage gate with $L = 20$ nm and $K_{uv} = 1.22 - 1.31$ MJ/m³ driven by a current of $J = 250$ MA/cm², in which the magnetization distributions of initial skyrmion bags are also shown. (b) Snapshots of skyrmion bag S(4) at different moments in the process of passing through three voltage gates (marked as gate1, gate2, and gate3) with $L = 20$ nm and $K_{uv} = 1.27$ MJ/m³ driven by a current of $J = 250$ MA/cm². $F_{i\perp}$ is the component of the force F_i ($i = 1, 3$) on inner antiskyrmions in the y direction. (c) Total energy variation of skyrmion bag S(4) in the process of passing through the voltage gates, where ΔE_1 , ΔE_2 , and ΔE_3 denote the energy gaps in the stable state between S(4) and S(3), S(3) and S(2), and S(2) and S(1), respectively. ($\Delta E_1 = 4.15 \times 10^{-19}$ J, $\Delta E_2 = 4.39 \times 10^{-19}$ J, and $\Delta E_3 = 4.92 \times 10^{-19}$ J).

different. The voltage gate is only 20 nm long but induces a maximum PMA of 1.27 MJ/m^3 , so it produces a large resistance to the skyrmion bag. When $t = 1.30 \text{ ns}$, a_4 is obstructed in gate2, so it gets closer to a_1 and a_3 , and it is squeezed by $F_{1\perp} + F_{2\perp}$ in the y direction and annihilated. Therefore, when S(3) passes gate2, a_4 is relatively easier to be annihilated than a_1 and a_3 . As discussed above, a_1 and a_3 are subjected to the same magnitude of repulsive forces and either pass through the voltage gate or be annihilated at the same time, so it is difficult to convert from S(3) to S(1). Finally, when S(2) passes through gate3, it only blocks a_1 and allows a_3 to pass, and S(1) formed can still remain its original shape due to its excellent topological protection. In Fig. 4(c), the energy gap ΔE_i ($i = 1-3$) between S(N) and S(N-1) ($N = 2-4$) still satisfies $\Delta E_1 < \Delta E_2 < \Delta E_3$ after the skyrmion bag reaches the stable state, and the energy of each inner antiskyrmion is still on the order $10^{-19} J$, which is consistent with our previous results.

IV. CONCLUSIONS

In conclusion, we have proposed a high-density racetrack memory based on skyrmion bags driven by STT in a synthetic antiferromagnetic racetrack with VCMA and investigated the mechanism of topological transformation of skyrmion bags. We have found the transitions from S(4) to S(N) ($N = 1-4$) can be controlled by adjusting the length of the voltage gate, PMA gradient within the voltage gate and driving current density, and the reason is related to the time of the skyrmion bags passing through the voltage gate and the repulsive forces between antiskyrmions inside the skyrmion bags. By comparing the energy gaps between S(N) and S(N-1) ($N = 1-4$) in the stable state, the energy of each inner antiskyrmion is on the order of $10^{-19} J$. We have further demonstrated that a series of continuous topological transitions from S(4) to S(1) can be realized by placing three voltage gates on a racetrack. This work is beneficial to the application of high-density racetrack memory and logical device based on skyrmion bags.

SUPPLEMENTARY MATERIAL

See the [supplementary material](#) for more results on the anisotropy curve along the racetrack, the magnetization distribution and energy variation of different arrangements of antiskyrmions inside skyrmion bag S(N).

AUTHOR DECLARATIONS

Conflict of Interest

The authors have no conflicts to disclose.

Author Contributions

Zhiyu Zhang: Conceptualization (equal); Data curation (equal); Investigation (equal); Software (equal); Visualization (equal). **Min Xu:** Supervision (equal); Writing – review & editing (equal). **Guiqian Jiang:** Software (equal); Visualization (equal). **Jinyu Zhang:** Resources (equal); Software (equal); Visualization (equal). **Dexiang Meng:** Resources (equal); Software (equal). **Wenlong Chen:** Resources (equal); Visualization (equal). **Yuliang Chen:**

Resources (equal); Visualization (equal). **Changjing Hu:** Software (equal); Visualization (equal).

DATA AVAILABILITY

The data that support the findings of this study are available from the corresponding author upon reasonable request

REFERENCES

- J. Sampaio, V. Cros, S. Rohart, A. Thiaville, and A. Fert, *Nat. Nanotechnol.* **8**, 839 (2013).
- G. Yu, P. Upadhyaya, Q. Shao, H. Wu, G. Yin, X. Li, C. He, W. Jiang, X. Han, P. K. Amiri, and K. L. Wang, *Nano Lett.* **17**, 261 (2017).
- L. Peng, K. Karube, Y. Taguchi, N. Nagaosa, Y. Tokura, and X. Yu, *Nat. Commun.* **12**, 6797 (2021).
- U. K. Rößler, A. N. Bogdanov, and C. Pfleiderer, *Nature* **442**, 797 (2006).
- A. Hrabec, J. Sampaio, M. Belmeguenai, I. Gross, R. Weil, S. M. Chérif, A. Stashkevich, V. Jacques, A. Thiaville, and S. Rohart, *Nat. Commun.* **8**, 15765 (2017).
- S. Mühlbauer, B. Binz, F. Jonietz, C. Pfleiderer, A. Rosch, A. Neubauer, R. Georgii, and P. Böni, *Science* **323**, 915, (2009).
- W. Kang, Y. Huang, C. Zheng, W. Lv, N. Lei, Y. Zhang, X. Zhang, Y. Zhou, and W. Zhao, *Sci. Rep.* **6**, 23164 (2016).
- A. Fert, V. Cros, and J. Sampaio, *Nat. Nanotechnol.* **8**, 152 (2013).
- X. Zhang, G. P. Zhao, H. Fangohr, J. P. Liu, W. X. Xia, J. Xia, and F. J. Morvan, *Sci. Rep.* **5**, 7643 (2015).
- R. Tomasello, E. Martinez, R. Zivieri, L. Torres, M. Carpentieri, and G. Finocchio, *Sci. Rep.* **4**, 6784 (2015).
- H. Xia, C. Song, C. Jin, J. Wang, J. Wang, and Q. Liu, *J. Magn. Magn. Mater.* **458**, 57 (2018).
- L. Shen, J. Xia, G. Zhao, X. Zhang, M. Ezawa, O. A. Tretiakov, X. Liu, and Y. Zhou, *Appl. Phys. Lett.* **114**, 042402 (2019).
- S. Zhang, J. Wang, Q. Zheng, Q. Zhu, X. Liu, S. Chen, C. Jin, Q. Liu, C. Jia, and D. Xue, *New J. Phys.* **17**, 023061 (2015).
- F. Garcia-Sanchez, J. Sampaio, N. Reyren, V. Cros, and J.-V. Kim, *New J. Phys.* **18**, 075011 (2016).
- J. Wang, J. Xia, X. Zhang, X. Zheng, G. Li, L. Chen, Y. Zhou, J. Wu, H. Yin, R. Chantrell, and Y. Xu, *Appl. Phys. Lett.* **117**, 202401 (2020).
- X. Zhang, Y. Zhou, M. Ezawa, G. P. Zhao, and W. Zhao, *Sci. Rep.* **5**, 11369 (2015).
- X. Zhang, M. Ezawa, and Y. Zhou, *Sci. Rep.* **5**, 9400 (2015).
- X. Xing, P. W. T. Pong, and Y. Zhou, *Phys. Rev. B* **94**, 054408 (2016).
- B. W. Walker, C. Cui, F. Garcia-Sanchez, J. A. C. Incorvia, X. Hu, and J. S. Friedman, *Appl. Phys. Lett.* **118**, 192404 (2021).
- Q. Sheng, X. L. Liu, W. J. Chen, M. Y. Li, L. J. Liu, and Y. Zheng, *J. Appl. Phys.* **125**, 064502 (2019).
- H. Zhang, D. Raftrey, Y.-T. Chan, Y.-T. Shao, R. Chen, X. Chen, X. Huang, J. T. Reichenadter, K. Dong, S. Susarla, L. Caretta, Z. Chen, J. Yao, P. Fischer, J. B. Neaton, W. Wu, D. A. Muller, R. J. Birgeneau, and R. Ramesh, *Sci. Adv.* **8**, eabm7103 (2022).
- D. Foster, C. Kind, P. J. Ackerman, J.-S. B. Tai, M. R. Dennis, and I. I. Smalyukh, *Nat. Phys.* **15**, 655 (2019).
- Z. Zeng, C. Zhang, C. Jin, J. Wang, C. Song, Y. Ma, Q. Liu, and J. Wang, *Appl. Phys. Lett.* **117**, 172404 (2020).
- C. Kind, S. Friedemann, and D. Read, *Appl. Phys. Lett.* **116**, 022413 (2020).
- Z. Zeng, C. Song, J. Wang, and Q. Liu, *J. Phys. D: Appl. Phys.* **55**, 185001 (2022).
- C. Kind and D. Foster, *Phys. Rev. B* **103**, L100413 (2021).
- M. J. Donahue and D. G. Porter, OOMMF User's Guide, Version 1.0, Interagency Report NIST IR 6376, Gaithersburg, MD (1999).
- S. Zhang and Z. Li, *Phys. Rev. Lett.* **93**, 127204 (2004).

²⁹X. Chen, W. Kang, D. Zhu, X. Zhang, N. Lei, Y. Zhang, Y. Zhou, and W. Zhao, *Appl. Phys. Lett.* **111**, 202406 (2017).

³⁰P. J. Hsu, A. Kubetzka, A. Finco, N. Romming, K. von Bergmann, and R. Wiesendanger, *Nat. Nanotechnol.* **12**, 123 (2017).

³¹D. M. Crum, M. Bouhassoune, J. Bouaziz, B. Schwefflinghaus, S. Blügel, and S. Lounis, *Nat. Commun.* **6**, 8541 (2015).

³²C. C. I. Ang, W. Gan, and W. S. Lew, *New J. Phys.* **21**, 043006 (2019).